参赛队员姓名： 刘天辰，袁子晨，莫晗琦

中学： 南京外国语学校

省份： 江苏省

国家/地区： 中国

指导教师姓名： 许亮亮，陈晓君

论文题目： **Cu-based metal-organic frameworks HKUST-1 as an effective catalyst for highly sensitive determination of ascorbic acid**

Cu-based metal-organic frameworks HKUST-1 as an effective catalyst for highly sensitive determination of ascorbic acid

Group Members

Tianchen Liu[1], Zichen Yuan[1], Hanqi Mo[2]

Instructor

Liangliang Xu, Xiaojun Chen

School

1. Nanjing Foreign Language School

2. Nanjing No.1 Middle School

Location

Nanjing, Jiangsu, P. R. China

Sep. 15, 2019

Abstract

In this work, a Cu-based nanosheet metal-organic framework, HKUST-1, was synthesized by using solvent method at room temperature. Its morphology and structure were characterized by scanning electron microscopy (SEM), transmission electron microscopy (TEM), energy dispersive X-ray spectroscopy (EDS), power X-ray diffraction (XRD), Fourier transform infrared (FT-IR) and Raman spectroscopy, respectively. The HKUST-1 was dripped and dried on the surface of indium tin oxide (ITO) electrode as modification material to carry out the electrochemical oxidation of ascorbic acid (AA). A two-electron-and-two-proton mechanism was deduced from the study on the pH of buffer solution, and a diffusion-controlled reaction process was confirmed by the dynamic calculation. In the case of optimization, the anionic current at + 0.02 V showed a linear relationship with the concentration of AA increasing within the range of 0.01-25 mM and 25-265 mM respectively. The limit of detection (LOD) was 3 μM (S/N = 3). The superb response could be attributed to the layer-by-layer and porous structure of HKUST-1, enhancing both the effective surface area and the electron transfer ability significantly. Moreover, the novel AA sensor verified fine reproducibility, high sensitivity and favorable stability towards glucose, uric acid (UA), several amino acids and dopamine (DA). It was successfully applied to the real sample testing of various tablets.

CONTENT

1. Introduction

Ascorbic acid (AA), also known as Vitamin C, is a polyhydroxy compound with similar structure with glucose [1]. It has a powerful and strong reducibility [2-4], widely used as a natural antioxidant in food [5], juice [6], medicine [4] and cosmetics [7]. It is also an vital water-soluble vitamin, which exists extensively as a highly active species participating in the metabolic processes of many creatures [8], fresh fruit and vegetables [6]. Recently, due to the crucial functions in free radical scavenging [3-5], cell development and therapeutic areas, such as wound healing, preventing cancer and enhancing immunity [9], AA has continuously attracted the public's interests. It was reported that AA shortage would lead to symptoms of scurvy [10], however, exaggerated amount would induce stomach convulsions [11]. Hence, the determination of the AA concentration is of great significance, which could be considered as an important physiological indicator for anti-aging [12-14]. Additionally, because AA is in a millimole or even smaller scale, particularly in human bodies, novel facile and rapid methods contributing to detecting selectively and sensitively are required. This is exactly significant not only for monitoring human metabolism, but also for the supervision of food, drugs and dietary supplement [15].

Nowadays, multitudinous methods have been applied to improve the determination of AA, including ultra- and high-performance liquid chromatography (UPLC, HPLC) [16-18], capillary electrophoresis [19], fluorescence spectroscopy [20] and UV-Vis spectroscopy [21]. Beyond these, electrochemical techniques are regularly applied, which are easy to operate and not expensive [22]. With the electrode surface modified, the electrochemical response could be promoted enormously and accessible to lower limit of detection (LOD) and wider linear range [23]. Nevertheless, the sensitivity and reproducibility usually tend to be the issue because of interference from other biological molecules like dopamine (DA) and uric acid (UA), leading to the challenge of employment in food, drug or real sample analysis [23].

Recently, numerous nanomaterials, for instance, graphene, carbon nanotubes (CNTs) [24] and nanoparticles (NPs) [25], have been developed and applied into electrochemical areas. Metal-organic frameworks (MOFs) are novel functional materials composed of repeated spatial or planar patterns of metal ions coordinated to organic ligands through covalent bonds. They have receiving more and more attention owing to the crucial role in the field of molecular adsorption [26], carbon capture [27], compound separation [28], supercapacitors [29], efficient sensing [30] and catalysis [31, 32] due to adjustable porous structures and superhigh specific areas. In electrochemical analysis, design and synthesis of different types of MOFs has become an appealing domain to study. It is reported that metal-organic frameworks are well electrochemically active to the oxidation of some small molecules such as glucose [33], nitrite [34], ethanol [35], hydrazine [36], dihydroxybenzene isomers [37], and the redox process of NADH [38] and H_2O_2 [33, 39, 40]. However, MOFs are rare as electrochemical sensors compared to others, because the organic coordinates are normally nonconductors and only the metal sites are conductive [40, 41]. Hence, it is challenging to prepare highly conductive electrochemical sensors based on MOFs.

To the best of our knowledge, none study has been reported so far on determining the concentration of AA using MOFs-modified electrodes. In this work, with 1,3,5-benzenetricarboxylic acid (H_3BTC) as the ligand and copper ion as the metal center, the prevalent HKUST-1 framework (also known as MOF-199 or Cu-BTC) was assembled at room temperature. Then the nanosheet structure was characterized and observed. In order to acquire the capability for electrochemical catalysis, the oxidation of AA was conducted using indium tin oxide (ITO) electrodes with HKUST-1 dripped onto the surface. The reaction surroundings, including pH, modification amount and scan rate, were researched as optimization, meanwhile the repeatability, interference and stability of AA were studied. Eventually, the novel detection platform was also tested by several health care tablets as standard samples.

2. Experimental

2.1 Chemicals

Ethanol acetone, copper(II) acetate monohydrate ($Cu(CH_3COO)_2 \cdot H_2O$), 1,3,5-benzenetricarboxylic acid (H_3BTC), dimethylformamide (DMF), cyclohexane, triethylamine, phosphoric acid (H_3PO_4), disodium phosphate (Na_2HPO_4), monosodium phosphate (NaH_2PO_4), magnesium chloride ($MgCl_2$), potassium chloride (KCl), potassium ferrocyanide ($K_4[Fe(CN)_6]$), potassium ferricyanide ($K_3[Fe(CN)_6]$), AA, uric acid (UA), dopamine (DA), glucose, glycine (Gly), L-Methionine (L-Met), L-Glutamic Acid (L-Glu), tryptophan (Trp), L-Cysteine (L-Cys), cystine (Cys-Cys) and tyrosine (Tyr). Real AA samples, including vitamin C honeysuckle pills, vitamin C buccal tablets for children and sweet-orange multi-vitamin effervescent tablets, were obtained from the market. The water was double distilled water (DDW) and all the chemicals were of analytical grade and used as received.

2.2 Apparatus

The morphology of the HKUST-1 was observed by scanning electron microscopy (SEM, Hitachi S4800) and transmission electron microscopy (TEM, JEOL JEM-200CX). The elemental composition analysis was investigated by energy dispersive X-ray spectroscopy (EDS Falcon 60S, EDAX Inc.). The power X-ray diffraction (XRD) pattern was performed by PhilipX'Pert X-ray diffractometer with Cu Kr X-ray source to characterize the crystal structure of HKUST-1. The bonding and functional groups were recorded using Fourier-transform infrared spectra (Nicolet iS 10 FT-IR spectrophotometer, Thermo Fisher Scientific Inc., USA) and Raman spectra (DXR2 Raman Microscope, Thermo Fisher Scientific Inc., USA). All the cyclic voltammetry (CV) and differential pulse voltammetry (DPV) measurements were performed on the electrochemical workstation (CHI650E, Shanghai Chen-hua

Instrument Co., China). A typical three-electrode system was applied in 0.1 M PBS at room temperature, composed of a HKUST-1-modified ITO working electrode, an Ag/AgCl reference electrode and a platinum wire auxiliary electrode.

2.3 Preparation of HKUST-1

HKUST-1 was synthesized at indoor temperature as previously reported [41, 42]. 0.60 g of $Cu(CH_3COO)_2 \cdot H_2O$ was dissolved in 50 mL of water and 0.42 g of H_3BTC was dissolved in 50 mL of ethanol, respectively. After they were completely merged, the mixture of 10 mL of cyclohexane with 0.85 mL of triethylamine was added dropwise to the surface of the solution. Then blue solid formed and precipitated sequentially. The reaction was allowed standing for 24 h before the solid was centrifugalized and filtered. The product was washed with distilled water and then followed by ethanol, and dried in vacuo at 50 °C for 12 h. It was stored in ethanol at 5 °C ready for use.

2.4 Fabrication of HKUST-1 modified ITO electrodes

Typically, 10 mg of HKUST-1 was added into 5 mL of DMF with ultrasonic oscillation for half an hour to obtain 2.0 mg mL^{-1} stable suspension. All the ITO electrodes were washed by acetone followed by ethanol and water. After the surfaces were dried under nitrogen, 7.0 μL of the suspension was dripped onto the controlled surface area of 1.0 cm^2, and then dried in air atmosphere [43].

3 Results and discussion

3.1 Characterization of HKUST-1

The morphology of the prepared HKUST-1 was illustrated by SEM and TEM. Fig.

1A, the SEM image, shows that this kind of metal-organic frameworks contained irregularly-layered sheet structures with smooth surfaces. The detailed structure could be clearly observed from the TEM image. As shown in Fig. 1B, the average thickness measurement of the sheets was evaluated about 150 nm. The large space in between increased the specific area of the material greatly, which would improve the electron-transfer efficiency when the nanosheets were loaded on the ITO electrode.

The chemical formula was calculated by EDS analysis in Fig. 1C. It is obvious that the molar ratio of the elements C, O and Cu of the prepared HKUST-1 was 53.38:36.98:9.64. This suggests that the metal-organic framework has a formula of $Cu_3(C_9H_3O_6)_2$ with an elemental ratio of C, O and Cu 6:4:1. It means that every three copper ions coordinated with two 1,3,5-benzenetricarboxylate linkers on average during the precipitation [41].

The powder XRD patterns of the synthesized HKUST-1 were compared with the simulated patterns through Crystal Diffract 6.7 [44, 45], as shown Fig. 1D. It indicated that the strong peaks at $2\theta = 6.38, 9.14, 11.26$ and $13.08°$ were identical to the calculated ones, corresponding to the (002), (022), (222) and (004) planes of HKUST-1, respectively. Therefore, the regular crystal structure of HKUST-1 was confirmed.

Moreover, the bonding of HKUST-1 was studied through FTIR and Raman spectroscopy. In Fig. 1E, the C-H stretching on the benzene ring (3400 cm^{-1}), the C=C stretching of the benzene ring (1619 and 1375 cm^{-1}), the vibration modes of asymmetric and symmetric $C-O_2$ (1571 and 1446 cm^{-1}) and the C-H bending (731 cm^{-1}) were clearly indicated. Apart from the organic fragments, the Cu-Cu vibration band, a homoatomic metal bond, was observed at 480 cm^{-1} by using the Raman spectrum in Fig. 1F. This corresponded to the crystal structure of HKUST-1 described in the earlier work [41].

Additionally, the structure of the nanosheets was stable during growing, assembling and precipitating at indoor temperature. The morphology remained after prolonged centrifugal separation and ultrasonic oscillation.
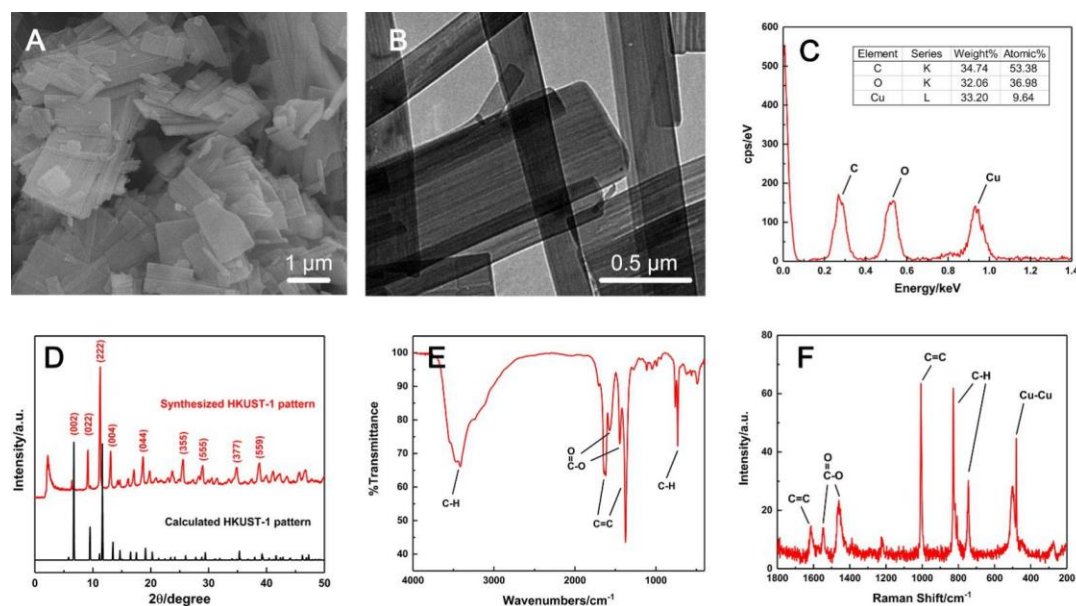
Fig. 1. (A) SEM and (B) TEM images of the synthesized HKUST-1; (C) EDS spectrum of the synthesized HKUST-1; (D) XRD patterns of the synthesized HKUST-1 and its homologous simulation; (E) FTIR and (F) Raman spectra of the synthesized HKUST-1.

3.2 Electrochemical behaviour of HKUST-1

The electrochemical behaviour of the HKUST-1-modified ITO electrode was studied using cyclic voltammetry (CV) before it was applied to the detection of AA (AA). Fig. 2 gives the response of ITO and HKUST-1/ITO in 0.1 M pH 3.63 PBS solution without AA at the scan rate of 100 mV s^{-1}. There were none obvious responses for the bare ITO electrode due to none electroactive material on its surface. However, for the modified electrode, the CV curve shows that the oxidation and reduction peaks were at +0.072 V and -0.240 V respectively, corresponding to the conversion between copper metal and copper (II) ion. The main difference is that the addition of metallic copper centers and the space between nanosheets enhanced the transfer of electrons greatly, increasing the current dramatically.
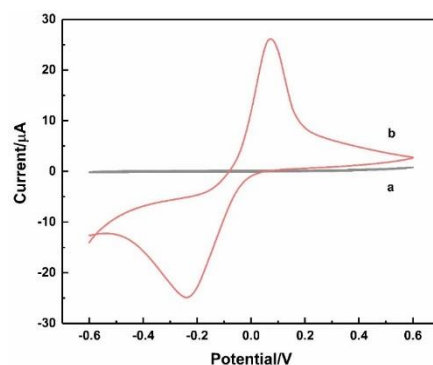
Fig. 2. CVs of bare ITO (a) and HKUST-1/ITO (b) in 0.1 M pH 3.63 PBS solution without AA at the scan rate of 100 mV s^{-1}.

3.3 Electrocatalytic oxidation of AA

Fig. 3 depicts different CV responses of bare ITO (a and a') and HKUST-1/ITO (b and b') in 0.1 M pH 3.63 PBS solution in the absence (a and b) and presence (a' and b') of 200 mM AA at the scan rate of 100 mV s^{-1}. Comparison of curves a and a' reveals no evidence for the catalytic effect of the bare ITO on the oxidation of AA. But from curves b and b', where the oxidation peak current increased two-fold with AA present, HKUST-1 was able to catalyze the oxidation of AA electrochemically. Furthermore, a possible mechanism would focus on the interaction between AA and HKUST-1. AA was oxidized to raise the current that did not appear on the bare electron, which overlapped with the oxidation peak of the modification material. As a result, the value of the current almost doubled. Meanwhile, the lost electrons from the oxidation of AA improved the reduction of some HKUST-1, facilitating the reduction peak slightly. The shoulder part was speculated to be attributed to the reduction of AA itself.
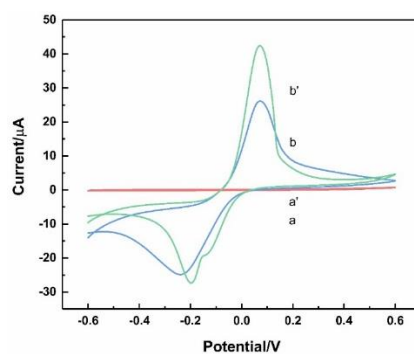
Fig. 3. CVs of bare ITO (a and a') and HKUST-1/ITO (b and b') in 0.1 M pH 3.63 PBS solution without AA (a and b) and with 200 mM AA (a' and b') at the scan rate of 100 mV s^{-1}.

3.4 Effect of solution pH

Fig. 4 shows the behaviour of HKUST-1/ITO in 0.1 M PBS solution with different pH values ranging from 3.00 to 6.31 in 1.0 mM AA present by using CV analysis. It is undoubted that the electrochemical responses of HKUST-1/ITO depended on the pH value of the buffer solution. Among the range of pH 3.00 to 6.31, the oxidation peak tended to moved towards more negative potentials as pH elevated. Fig. 4A showed the linear plot of oxidation potential of AA versus pH values, expressed by the fitting equation $E_{pa}/V = -0.0494 \, pH + 0.3040$ ($R^2 = 0.9933$). This gave evidence for more available oxidation of AA with increasing alkali in the solution, indicating that the deprotonation step was involved in the oxidation. In addition, the slope, -49.4 mV/pH, was coming close to the theoretical value, -59 mV/pH, for a process transferring two electrons and two protons deduced by the Nernst equation

$$\frac{dE_p}{dpH} = \frac{-2.303mRT}{nF} \,,$$

where m represent the number of protons and n represent the number of electrons involved in the reaction. Hence, the mechanism should be as the following scheme [46, 47]:
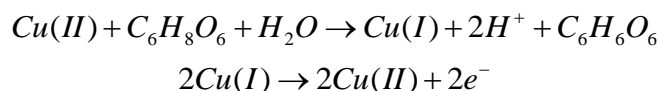
$$Cu(II) + C_6H_8O_6 + H_2O \rightarrow Cu(I) + 2H^+ + C_6H_6O_6$$
$$2Cu(I) \rightarrow 2Cu(II) + 2e^-$$

Fig. 4B is the plot of I_{pa} versus pH. Obviously, the oxidation current of AA displayed a steep raise first, achieving the highest peak current at pH 3.63. Then, the current decreased rapidly as pH elevated from 3.63 to 6.31. Therefore, the study of the pH effect suggested that pH 3.63 should be taken as the optimum analysis condition to ensure sufficient current responses.
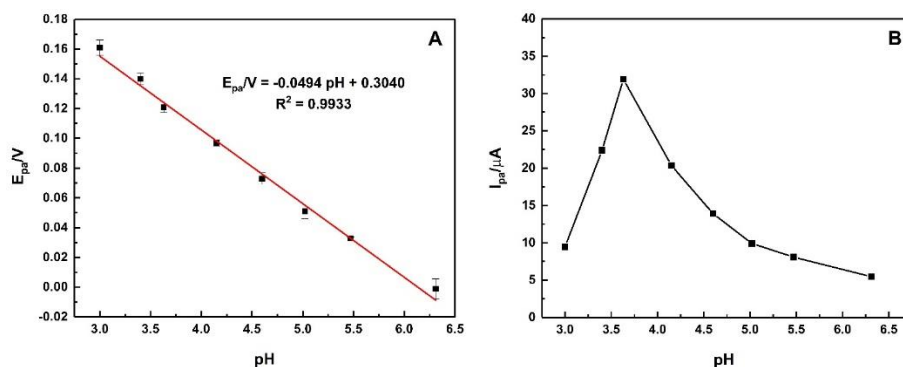
Fig. 4. Plot of (A) oxidation potential and (B) oxidation current versus pH from CVs of HKUST-1/ITO in 0.1 M PBS solution under different pH values ranging from 3.00 to 6.31 for 1.0 mM AA at the scan rate of 100 mV s^{-1}.

3.5 Effect of modification amount of HKUST-1

The influence of the modification material amount was studied using DPV as shown in Fig. 5. The modification amount did have great impacts on the current of the oxidation peak. It was found that the oxidation current of AA enhanced sharply when the volume of HKUST-1/DMF suspension was added from 1.5 to 7.0 μL, due to increasing active surface area for electron transfer. But the current suddenly reduced as the modification amount was up to 9.0 μL then. The main reason was a decrease in electric conductivity, caused by excessive metal-organic frameworks hindering the electrons reaching the electrode surface or reacting with the copper ions. As a result, 7.0 μL suspension of HKUST-1 was selected as the optimum modification amount for the detection of AA.
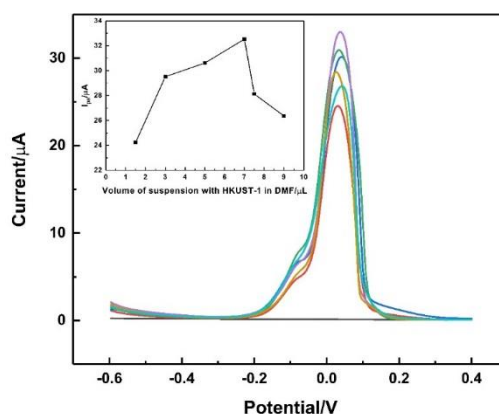

Fig. 5. DPVs of HKUST-1/ITO in 0.1 M pH 3.63 PBS solution for 1.0 mM AA at the scan rate of 100 mV s^{-1} with different volume of HKUST-1/DMF suspension from 1.5 to 9.0 μL. Inset: plot of I_{pa} versus modification amount.

3.6 Effect of scan rate

3.6.1 In PBS solution

The scan rate effect and the dynamics study were investigated by CV using HKUST-1/ITO in bare PBS solution without AA in the scan rate range of 30 - 200 mV s^{-1}. Fig. 6 illustrates the general tendency that the oxidation potential shifted towards the positive direction and the reduction one shifted negatively as the scan rate increased. The relationship between the potentials and the logarithm of scan rate was shown in Fig. 6(a) by the linear equation: E_{pa}/V = 0.1024 log(v/(mV s^{-1})) -0.0565 (R^2 = 0.9956) and E_{pc}/V = -0.1228 log(v/(mV s^{-1})) + 0.0225 (R^2 = 0.9901), respectively. Then, the dynamics-relating parameters could be determined using Laviron equation:

$$
\begin{cases}
E_{p,a} = E^{0'} + \dfrac{2.303RT \log v}{(1-\alpha)nF} & (1) \\[2ex]
E_{p,c} = E^{0'} - \dfrac{2.303RT \log v}{\alpha nF} & (2) \\[2ex]
\log k_s = \alpha \log(1-\alpha) + (1-\alpha)\log \alpha - \log \dfrac{RT}{nvF} - \dfrac{\alpha(1-\alpha)nF\Delta Ep}{2.303RT} & (3)
\end{cases}
$$

α, n and k_s were prescribed previously [48, 49]. From the slopes and intercepts in the linear equations, the value of α and n were calculated as 0.45 and 1.06, showing a single-electron process. When the scan rate was 100 mV s^{-1}, k_s was got as 0.0445 s^{-1}, and the large gap between E_{pa} and E_{pc} proved for an irreversible redox reaction. Meanwhile, both the current of anodic and cathodic peaks tended to have a great increase. As compared with Fig. 6(b) and (c), the anodic current fitted better with the square root of scan rate v$^{1/2}$ than with the scan rate itself. The relationship was expressed as i_{pa}/μA = 1.6944 (v/(mV s^{-1}))$^{1/2}$ + 9.6844 (R^2 = 0.9955). Therefore, a diffusion-controlled electrochemical process was confirmed in the redox reaction of HKUST-1/ITO electrode in bare PBS solution.
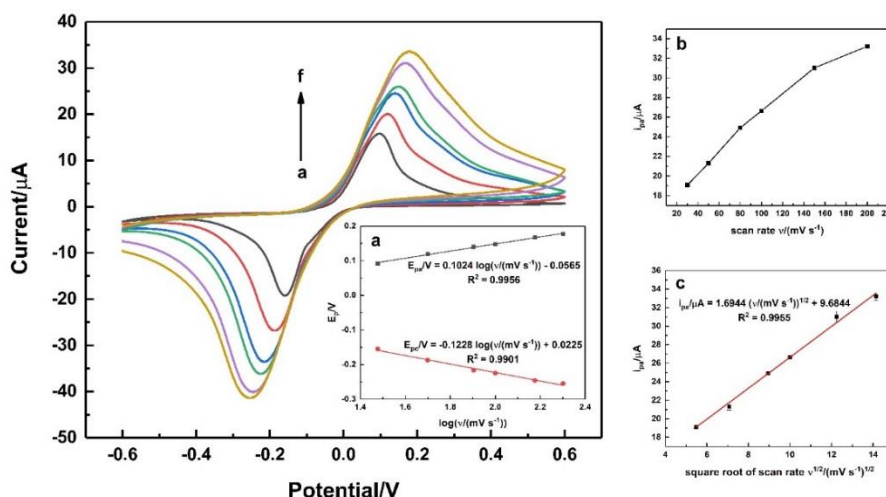
Fig. 6. CVs of HKUST-1/ITO in 0.1 M pH 3.63 PBS solution without AA at different scan rates of 30, 50, 80, 100, 150 and 200 mV s^{-1} (from a to f). (a) The linear plots of E_{pa} and E_{pc} vs. log v. (b) The curve plot of i_{pa} vs. v. (c) The linear plot of i_{pa} vs. $v^{1/2}$.

3.6.2 In Fe(CN)$_6^{3-/4-}$ solution

Fig. 7 illustrates the CVs of HKUST-1/ITO in 5 mM $K_3Fe(CN)_6$/$K_4Fe(CN)_6$ solution containing 0.1 M KCl at various scan rate. The curves were the combined results of the redox of HKUST-1 and Fe(CN)$_6^{3-/4-}$, with two oxidation peaks. The negative one corresponded to HKUST-1, while the positive one was oxidation from Fe(CN)$_6^{4-}$ to Fe(CN)$_6^{3-}$. But only one single broad reductive peak was observed because their reduction potentials were similar. Besides, the current for the reduction of HKUST-1 tended to be small, which overlapped with that of Fe(CN)$_6^{3-/4-}$.

Considering the redox behaviour of Fe(CN)$_6^{3-/4-}$, both the oxidation and reduction potentials shifted as the same way as HKUST-1 did in 3.6.1 as the scan rate increased, with the relationship in Fig. 7(a): E_{pa}/V = 0.07068 log(v/(mV s^{-1})) + 0.18887 (R^2 = 0.9970) and E_{pc}/V = -0.05391 log(v/(mV s^{-1})) + 0.05614 (R^2 = 0.9938). Likewise, dynamic parameters were calculated from the Laviron equation, giving α = 0.57, n = 1.93 and k_s (at 100 mV s^{-1}) = 0.0236 s^{-1}. As compared with the curves in Fig. 7(b) and (c) for the oxidation of Fe(CN)$_6^{3-/4-}$, the relationship between the oxidation current and $v^{1/2}$ could be fitted with the linear equation i_{pa}/μA = 3.4201 (v/(mV s^{-1}))$^{1/2}$ - 6.5569 (R^2 = 0.9913), indicating a diffusion-controlled step as well.

Furthermore, the effective surface area (ESA) could be deduced here. This is of

great importance because it influenced the accuracy and sensitivity through affecting the magnitude of the current. The effective area of the modified ITO electrode could be determined by Randles-Sevcike equation: $i_p = 2.69 \times 10^5 \, n^{3/2} \, A \, D^{1/2} \, v^{1/2} \, C$, where i_p (A) is the peak current in an oxidation or reduction process, n is the number of electrons involved in the reaction, A (cm^2) is the effective surface area, D ($cm^2 \, s^{-1}$) is the diffusion coefficient of $Fe(CN)_6^{3-}$ (6.5×10^{-6} $cm^2 \, s^{-1}$), C (mol cm^{-3}) is the concentration of the molecule $Fe(CN)_6^{3-}$ in the solution (2.5 mM) and v (V s^{-1}) is the scan rate [50]. In this case, the ESA of HKUST-1/ITO was 0.06308 cm^2, which was 7.83 times of that of an unmodified ITO electrode, 8.06×10^{-3} cm^2. This indicated that the modification material HKUST-1 could enhance the electron transfer by providing greater electroactive surface area.
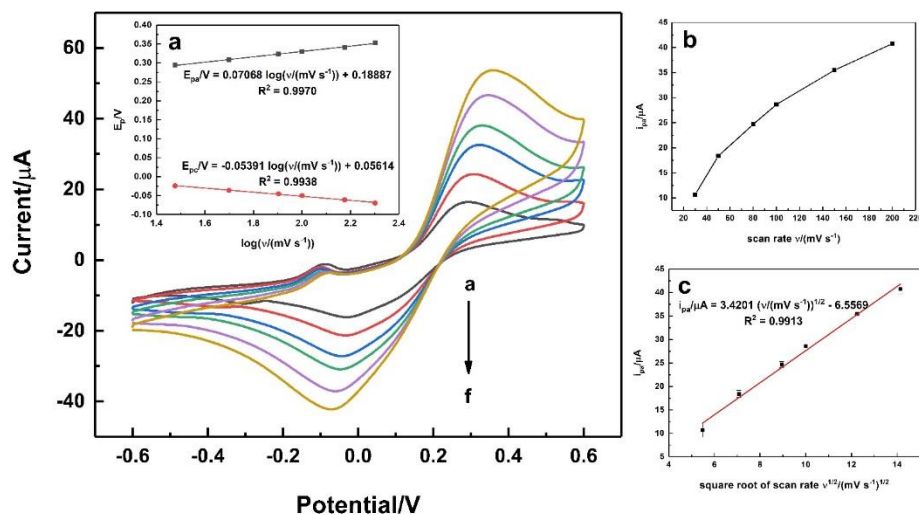

Fig. 7. CVs of HKUST-1/ITO in 2.5 mM $K_3Fe(CN)_6$/2.5 mM $K_4Fe(CN)_6$ solution containing 0.1 M KCl without AA at different scan rate of 30, 50, 80, 100, 150 and 200 mV s^{-1} (from a to f). (a) The linear plots of E_{pa} and E_{pc} vs. log v. (b) The curve plot of i_{pa} vs. v. (c) The linear plot of i_{pa} vs. $v^{1/2}$.

3.6.3 In AA solution

The effectiveness of the scan rate on the electrocatalytic oxidation of AA was also investigated. Fig. 8 gives CVs of the modified electrode within 0.1 M pH 3.63 PBS solution containing 1.0 mM AA recorded at different scan rate. The tendency of the changes on peak potential in the previous sections also applied here, and the fitting

relationship was $E_{pa}/V = 0.0458 \log(v/(mV\ s^{-1})) + 0.0279$ ($R^2 = 0.9918$) and $E_{pc}/V = -0.0811 \log(v/(mV\ s^{-1})) + 0.0081$ ($R^2 = 0.9941$), respectively. Thus, the electron-transfer number (n) in rate determining step was calculated as 2.02 using Laviron equation, proving the two-electron-and-two-proton mechanism. Furthermore, the electron-transfer coefficient (α) was 0.36 and the reaction rate constant (k_s) was 0.0246 s^{-1} at 100 mV s^{-1}. In addition, both the anodic and cathodic current showed linear relationship with the square root of scan rate, which were $i_{pa}/\mu A = 0.7003 (v/(mV\ s^{-1}))^{1/2} + 23.7727$ ($R^2 = 0.9089$) and $i_{pc}/\mu A = -1.4796 (v/(mV\ s^{-1}))^{1/2} - 0.7818$ ($R^2 = 0.9987$), illustrating a diffusion-controlled process.
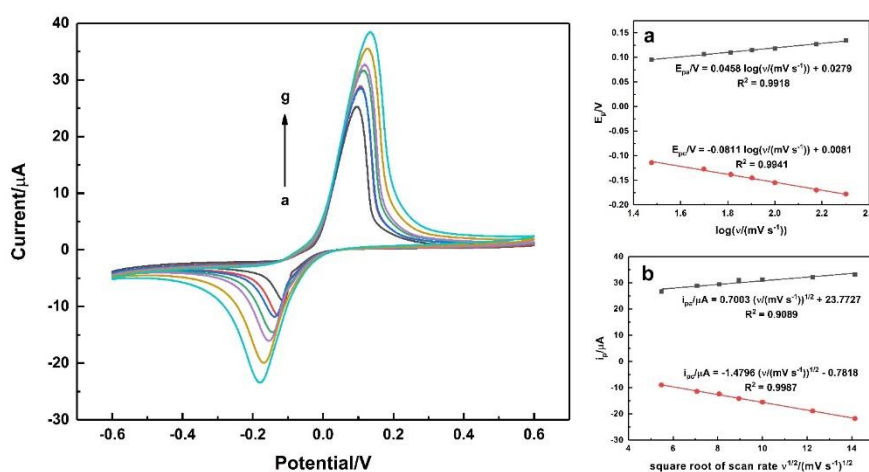

Fig. 8. CVs of HKUST-1/ITO in 0.1 M pH 3.63 PBS solution containing 1.0 mM AA at different scan rate of 30, 50, 65, 80, 100, 150 and 200 mV s^{-1} (from a to g). (a) The linear plots of E_{pa} and E_{pc} vs. log v. (b) The linear plots of i_{pa} and i_{pc} vs. $v^{1/2}$.

3.7 Electrochemical detection of AA

The elecrtrocatalytic responses of AA at different concentrations on HKUST-1/ITO were examined using DPV technique. The optimized condition was implemented which was 0.1 M of pH 3.63 PBS solution, the scan rate of 100 mV s^{-1} and the suspension volume of 7.0 µL. As shown in Fig. 9, the oxidation current increased in a micron level when AA was added successively in a scale of millimole from 0.01 to 265 mM, while the peak potential kept around +0.02 V. The linear range was composed of two parts. The first part was at a low concentration range of 0.01-25 mM, where the current grew rapidly and the regression equation was $\Delta I/\mu A = 0.5098\ C_{AA}/mM + 2.6901$ ($R^2 = 0.9949$, n = 6). The other one was at a high concentration range of 25-265 mM, but the current increased in a smaller slope than before. The linear relationship was $\Delta I/\mu A = 0.1444\ C_{AA}/mM + 11.3245$ ($R^2 = 0.9967$, n = 9).

Overall, the limit of detection was obtained as 3 μM (S/N=3). Compared with the previously reported works determining the concentration of AA listed in Table 1, this platform of electrochemical sensor revealed a wider linear range and a lower limit of detection. This would be mainly attributed to the higher effective surface area of HKUST-1 nanosheets and thus more vacant sites available for the electrocatalytic oxidation.
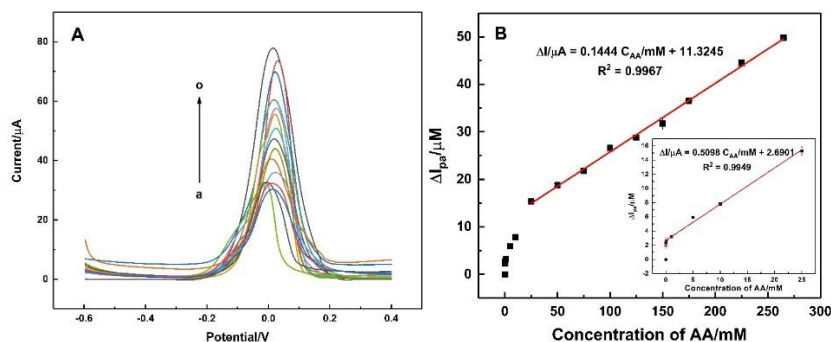

Fig. 9. (A) DPVs of HKUST-1/ITO in 0.1 M pH 3.63 PBS solution in the presence of AA at the scan rate of 100 mV s^{-1}. AA concentrations: 0, 0.01, 0.1, 1, 5, 10, 25, 50, 75, 100, 125, 150, 175, 225 and 265 mM (from a to o). (B) The calibration curve of ΔI_{pa} vs. AA at low concentrations and at high concentrations (inset).

Table 1. Comparisons with some previous works using different modified electrodes on the detection of AA.

AA sensor	Linear range /mM	Limit of detection /μM	Ref.
$Cu_4(OH)_6SO_4$/ITO	0.017-6	6.4	[46]
Pre-anodized inlaying ultrathin CPE	0.01-1.5	0.31	[22]
AuNPs@MoS_2/GCE	0.05-100	50	[51]
GEF/CFE	0.07-2.31	73.52	[52]
ZnO–Cu_xO–PPy/GCE	0.2-1	25.0	[53]
rGO–CNT/ITO	0.01-0.2	5.31	[54]
Pd@Au/rGO/GCE	0.05-2.86	24.88	[55]
AuNPs/PDDA/GNS/GCE	0.6-4.2	80	[56]
HNP-PtTi/GCE	0.2-1	24.2	[57]
PrGO/PB/GCE	0.283-2.33	34.7	[58]
HKUST-1/ITO	0.01-25 and 25-265	3	This

3.8 Repeatability, stability and selectivity of the sensor

The repeatability and stability were evaluated using the same working electrode for 15 continuous measurements of 1.0 mM AA in 0.1 M pH 3.63 PBS solution at the scan rate of 100 mV s^{-1}. The relative standard deviation (RSD) acquired was 2.18 %, showing favourable reproducibility. Additionally, the short-time and long-time stability were tested 7 and 21 days after the initial utilization. During this time, the modified electrodes were stored in 0.1 mM pH 3.63 bare PBS solution. Only 2.17 % and 6.91 % of the current responses were lost, respectively, thus indicating good stability.

The selectivity plays an essential role in the detection of real samples and gives a common way to investigate the sensitivity of an electrochemical system. Ten different types of interfering substances, including glucose, DA, UA, amino acid, etc., were examined at the concentration of 1.0 mM in the same PBS solution, and the results were shown in Fig. 10. Glucose, UA and DA contributed to raise the current, but only by less than 10 % of the current increased for AA. Contrarily, most of the amino acids reduced the current slightly. Both certified the highly sensitive electrochemical oxidation of AA with HKUST-1/ITO.
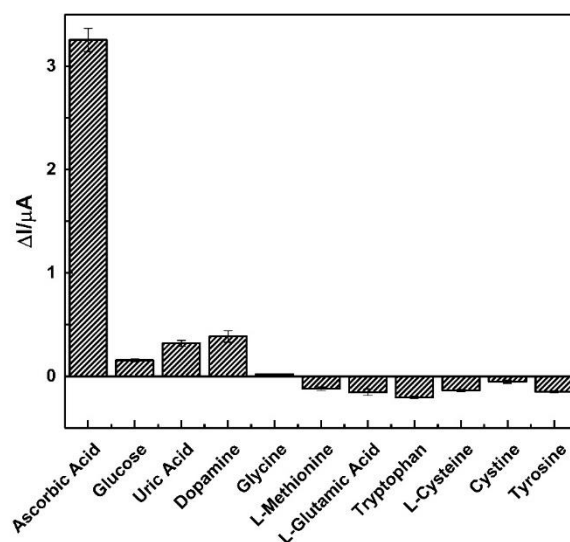

Fig. 10. Plot of ΔI in DPV curves towards 1.0 mM of ten interfering substances: glucose, uric acid, dopamine, glycine, L-methionine, L-glutamic acid, tryptophan, L-cysteine, cystine and tryosine.

3.9 Analytical application on real samples

In order to evaluate the practical performance of the new electrochemical AA sensor with HKUST-1/ITO, the proposed method was employed to various health care tablets. The results were listed below in Table 2. All of them were examined in 0.1 M pH 3.63 PBS solution at room temperature, and DPVs were recorded from -0.6 to 0.4 V. Additionally, each sample test was repeated triply, and the RSDs were lower than 5 %, showing a satisfying precision. The general recovery ranged between 99.5 % to 102.6 %, illustrating approved accuracy. Hence, it is feasible to complete the detection of AA concentration in this approach.

Table 2. Determination and recovery of AA in real samples.

Sample	Mass of AA contained/ mg	Volume of Solution/mL	Standard Concentration/ mM	$\Delta I/\mu A$	Measured Concentration/ mM	Recovery
Vitamin C honeysuckle pill	49.5	25	11.24	8.488	11.37	101.15 %
Vitamin C buccal tablet for children	60	25	13.63	9.603	13.56	99.51 %
Sweet orange multi-vitamin effervescent tablet	225	30	42.58	17.64	43.68	102.57 %

4 Conclusions

In summary, a typical type of Cu-based nanosheet metal-organic frameworks functioned as the modification material on the surface of the ITO electrode to form a novel electrochemical sensor for AA. It provided large effective surface area and improved the electron transfer ability significantly, thus resulting in great enhancement of the oxidation current towards AA. Then, effects on the pH of buffer solution, the amount of suspension and the scan rate were studied to find the optimized condition for AA detection, deduce the two-electron-and-two-proton mechanism and give evidence for the enhancement of electrocatalytic oxidation. The

novel sensor tended to exhibit a wide linear range (0.01-25 and 25-265 mM), low limit of detection (3 μM, S/N=3), favorable stability, fine reproducibility and high sensitivity. Furthermore, it was successfully applied to the real sample testing of various tablets.

References

[1] J. Hvoslef, The crystal structure of L-ascorbic acid, 'vitamin C'. II. The neutron diffraction analysis, Acta Crystallographica Section B, 24(1968) 1431-40.

[2] O. Arrigoni, M.C.D. Tullio, Ascorbic acid: much more than just an antioxidant, Biochim Biophys Acta, Gen Subj, 1569(2002) 1-9.

[3] N.A. Akram, F. Shafiq, M. Ashraf, Ascorbic Acid-A Potential Oxidant Scavenger and Its Role in Plant Development and Abiotic Stress Tolerance, Front Plant Sci, 8(2017) 613.

[4] M.G. Traber, J.F. Stevens, Vitamins C and E: beneficial effects from a mechanistic perspective, Free Radic Biol Med, 51(2011) 1000-13.

[5] E. Choe, D.B. Min, Mechanisms of Antioxidants in the Oxidation of Foods, Comprehensive Reviews in Food Science and Food Safety, 8(2009) 345-58.

[6] H. Wang, G.H. Cao, R.L. Prior, Total antioxidant capacity of fruits, Journal of Agricultural and Food Chemistry, 44(1996) 701-5.

[7] M. Gallarate, M.E. Carlotti, M. Trotta, S. Bovo, On the stability of ascorbic acid in emulsified systems for topical and cosmetic use, International Journal of Pharmaceutics, 188(1999) 233-41.

[8] D.R. Gallie, The role of L-ascorbic acid recycling in responding to environmental stress and in promoting plant growth, J Exp Bot, 64(2013) 433-43.

[9] B.A. Eipper, R.E. Mains, C.C. Glembotski, Identification in pituitary tissue of a peptide alpha-amidation activity that acts on glycine-extended peptides and requires molecular oxygen, copper, and ascorbic acid, Proc Natl Acad Sci USA, 80(1983) 5144-8.

[10] S.J. Padayatty, A. Katz, Y. Wang, P. Eck, O. Kwon, J.-H. Lee, et al., Vitamin C as an Antioxidant: Evaluation of Its Role in Disease Prevention, Journal of the American College of Nutrition, 22(2003) 18-35.

[11] M. Sonmez, G. Turk, A. Yuce, The effect of ascorbic acid supplementation on sperm quality, lipid peroxidation and testosterone levels of male Wistar rats, Theriogenology, 63(2005) 2063-72.

[12] G.C. de Menezes, M. Tavares-Dias, E.A. Ono, J.I. de Andrade, E.M. Brasil, R. Roubach, et al., The influence of dietary vitamin C and E supplementation on the physiological response of pirarucu, Arapaima gigas, in net culture, Comp Biochem Physiol A Mol Integr Physiol, 145(2006) 274-9.

[13] S. Gueguen, P. Pirollet, P. Leroy, J.-C. Guilland, J. Arnaud, F. Paille, et al., Changes in Serum Retinol, α-Tocopherol, Vitamin C, Carotenoids, Zinc and Selenium after Micronutrient Supplementation during Alcohol Rehabilitation, Journal of the American College of Nutrition, 22(2003) 303-10.

[14] S.E. Gariballa, A.J. Sinclair, Nutrition, ageing and ill health, British Journal of Nutrition, 80(2007).

[15] J. Ping, J. Wu, Y. Wang, Y. Ying, Simultaneous determination of ascorbic acid, dopamine and uric acid using high-performance screen-printed graphene electrode, Biosens Bioelectron, 34(2012) 70-6.

[16] A. Mazurek, J. Jamroz, Precision of dehydroascorbic acid quantitation with the use of the subtraction method--validation of HPLC-DAD method for determination of total vitamin C in food, Food Chem, 173(2015) 543-50.

[17] I. Klimczak, A. Gliszczynska-Swiglo, Comparison of UPLC and HPLC methods for determination of vitamin C, Food Chem, 175(2015) 100-5.

[18] Z. Chen, B. Chen, S. Yao, High-performance liquid chromatography/electrospray ionization-mass spectrometry for simultaneous determination of taurine and 10 water-soluble vitamins in multivitamin tablets, Analytica Chimica Acta, 569(2006) 169-75.

[19] T. Wu, Y. Guan, J. Ye, Determination of flavonoids and ascorbic acid in grapefruit peel and juice by capillary electrophoresis with electrochemical detection, Food Chemistry, 100(2007) 1573-9.

[20] M. Zheng, Z. Xie, D. Qu, D. Li, P. Du, X. Jing, et al., On-off-on fluorescent carbon dot nanosensor for recognition of chromium(VI) and ascorbic acid based on the inner filter effect, ACS Appl Mater Interfaces, 5(2013) 13242-7.

[21] B. Shyla, G. Nagendrappa, Redox spectrophotometric method involving electrolytically generated manganese(III) sulphate with diphenylamine for the determination of ascorbic acid present in the samples of various fruits, commercial juices and sprouted food grains, Food Chem, 138(2013) 2036-42.

[22] J. Wang, J.e. Huo, J. Li, E. Shangguan, Q. Li, Simultaneous determination of ascorbic acid and acetaminophen at the pre-anodized inlaying ultrathin carbon paste electrode, Analytical Methods, 5(2013).

[23] M. Sajid, M.K. Nazal, M. Mansha, A. Alsharaa, S.M.S. Jillani, C. Basheer, Chemically modified electrodes for electrochemical detection of dopamine in the presence of uric acid and ascorbic acid: A review, TrAC Trends in Analytical Chemistry, 76(2016) 15-29.

[24] S. He, Y. Yu, Z. Chen, Q. Shi, L. Zhang, Synergistic Effect of Graphene and Multiwalled Carbon Nanotubes on a Glassy Carbon Electrode for Simultaneous Determination of Uric Acid and Dopamine in the Presence of Ascorbic Acid, Analytical Letters, 48(2014) 248-58.

[25] E. Molaakbari, A. Mostafavi, H. Beitollahi, Simultaneous electrochemical determination of dopamine, melatonin, methionine and caffeine, Sensors and Actuators B: Chemical, 208(2015) 195-203.

[26] Q. Yang, Y. Wang, J. Wang, F. Liu, N. Hu, H. Pei, et al., High effective adsorption/removal of illegal food dyes from contaminated aqueous solution by Zr-MOFs (UiO-67), Food Chem, 254(2018) 241-8.

[27] M. Bui, C.S. Adjiman, A. Bardow, E.J. Anthony, A. Boston, S. Brown, et al., Carbon capture and storage (CCS): the way forward, Energy & Environmental Science, 11(2018) 1062-176.

[28] J.R. Li, R.J. Kuppler, H.C. Zhou, Selective gas adsorption and separation in metal-organic frameworks, Chem Soc Rev, 38(2009) 1477-504.

[29] M. Liu, F. Zhao, D. Zhu, H. Duan, Y. Lv, L. Li, et al., Ultramicroporous carbon nanoparticles derived from metal–organic framework nanoparticles for high-performance supercapacitors, Materials Chemistry and Physics, 211(2018) 234-41.

[30] H.R. Fu, Y. Zhao, Z. Zhou, X.G. Yang, L.F. Ma, Neutral ligand TIPA-based two 2D metal-organic frameworks: ultrahigh selectivity of C2H2/CH4 and efficient sensing and sorption of Cr(vi), Dalton Trans, 47(2018) 3725-32.

[31] J. Lee, O.K. Farha, J. Roberts, K.A. Scheidt, S.T. Nguyen, J.T. Hupp, Metal-organic framework materials as catalysts, Chem Soc Rev, 38(2009) 1450-9.

[32] J. Duan, S. Chen, C. Zhao, Ultrathin metal-organic framework array for efficient electrocatalytic water splitting, Nat Commun, 8(2017) 15341.

[33] D. Zhang, J. Zhang, R. Zhang, H. Shi, Y. Guo, X. Guo, et al., 3D porous metal-organic framework as an efficient electrocatalyst for nonenzymatic sensing application, Talanta, 144(2015) 1176-81.

[34] B. Yuan, J. Zhang, R. Zhang, H. Shi, N. Wang, J. Li, et al., Cu-based metal–organic framework as a novel sensing platform for the enhanced electro-oxidation of nitrite, Sensors and Actuators B: Chemical, 222(2016) 632-7.

[35] L. Yang, S. Kinoshita, T. Yamada, S. Kanda, H. Kitagawa, M. Tokunaga, et al., A metal-organic framework as an electrocatalyst for ethanol oxidation, Angew Chem Int Ed Engl, 49(2010) 5348-51.

[36] H. Hosseini, H. Ahmar, A. Dehghani, A. Bagheri, A.R. Fakhari, M.M. Amini, Au-SH-SiO2 nanoparticles supported on metal-organic framework (Au-SH-SiO2@Cu-MOF) as a sensor for electrocatalytic oxidation and determination of hydrazine, Electrochimica Acta, 88(2013) 301-9.

[37] Y. Yang, Q. Wang, W. Qiu, H. Guo, F. Gao, Covalent Immobilization of Cu3(btc)2 at Chitosan–Electroreduced Graphene Oxide Hybrid Film and Its Application for Simultaneous Detection of Dihydroxybenzene Isomers, The Journal of Physical Chemistry C, 120(2016) 9794-803.

[38] Y. Zhang, X. Bo, C. Luhana, H. Wang, M. Li, L. Guo, Facile synthesis of a Cu-based MOF confined in macroporous carbon hybrid material with enhanced electrocatalytic ability, Chem Commun (Camb), 49(2013) 6885-7.

[39] H. Dai, W. Lu, X. Zuo, Q. Zhu, C. Pan, X. Niu, et al., A novel biosensor based on boronic acid functionalized metal-organic frameworks for the determination of hydrogen peroxide released from living cells, Biosens Bioelectron, 95(2017) 131-7.

[40] L. Wang, H. Yang, J. He, Y. Zhang, J. Yu, Y. Song, Cu-Hemin Metal-Organic-Frameworks/Chitosan-Reduced Graphene Oxide Nanocomposites with Peroxidase-Like Bioactivity for Electrochemical Sensing, Electrochimica Acta, 213(2016) 691-7.

[41] L. Ji, Q. Cheng, K. Wu, X. Yang, Cu-BTC frameworks-based electrochemical sensing platform for rapid and simple determination of Sunset yellow and Tartrazine, Sensors and Actuators B: Chemical, 231(2016) 12-7.

[42] Y.V. Kaneti, J. Tang, R.R. Salunkhe, X. Jiang, A. Yu, K.C. Wu, et al., Nanoarchitectured Design of Porous Materials and Nanocomposites from Metal-Organic Frameworks, Adv Mater, 29(2017).

[43] H. Hosseini, H. Ahmar, A. Dehghani, A. Bagheri, A. Tadjarodi, A.R. Fakhari, A novel electrochemical sensor based on metal-organic framework for electro-catalytic oxidation of L-cysteine, Biosens Bioelectron, 42(2013) 426-9.

[44] V.K. Peterson, P.D. Southon, G.J. Halder, D.J. Price, J.J. Bevitt, C.J. Kepert, Guest Adsorption in the Nanoporous Metal–Organic Framework Cu3(1,3,5-Benzenetricarboxylate)2: Combined In Situ X-ray Diffraction and Vapor Sorption, Chemistry of Materials, 26(2014) 4712-23.

[45] C. Duan, F. Li, S. Luo, J. Xiao, L. Li, H. Xi, Facile synthesis of hierarchical porous metal-organic frameworks with enhanced catalytic activity, Chemical Engineering Journal, 334(2018) 1477-83.

[46] C. Xia, W. Ning, A novel bio-electrochemical ascorbic acid sensor modified with $Cu_4(OH)_6SO_4$ nanorods, Analyst, 136(2011) 288-92.

[47] F. Gao, L. Zhu, H. Li, H. Xie, Hierarchical flower-like CuO film: One-step room temperature synthesis, formation mechanism and excellent optoelectronic properties, Materials Research Bulletin, 93(2017) 342-51.

[48] E. Laviron, General expression of the linear potential sweep voltammogram in the case of diffusionless electrochemical systems, Journal of Electroanalytical Chemistry and Interfacial Electrochemistry, 101(1979) 19-28.

[49] L. Liu, C. Duan, Z. Gao, Electrochemical Behavior and Electrochemical Determination of Tiamulin Fumarate at an Ionic Liquid Modified Carbon Paste Electrode, Croatica Chemica Acta, 83(2010) 409-14.

[50] Y. Zhou, X. Ni, Z. Ren, J. Ma, J. Xu, X. Chen, A flower-like NiO–SnO2 nanocomposite and its non-enzymatic catalysis of glucose, RSC Advances, 7(2017) 45177-84.

[51] H. Sun, J. Chao, X. Zuo, S. Su, X. Liu, L. Yuwen, et al., Gold nanoparticle-decorated MoS2 nanosheets for simultaneous detection of ascorbic acid, dopamine and uric acid, RSC Advances, 4(2014).

[52] J. Du, R. Yue, F. Ren, Z. Yao, F. Jiang, P. Yang, et al., Novel graphene flowers modified carbon fibers for simultaneous determination of ascorbic acid, dopamine and uric acid, Biosens Bioelectron, 53(2014) 220-4.

[53] K. Ghanbari, N. Hajheidari, ZnO-CuxO/polypyrrole nanocomposite modified electrode for simultaneous determination of ascorbic acid, dopamine, and uric acid, Anal Biochem, 473(2015) 53-62.

[54] Y. Zhang, Y. Ji, Z. Wang, S. Liu, T. Zhang, Electrodeposition synthesis of reduced graphene oxide–carbon nanotube hybrids on indium tin oxide electrode for simultaneous electrochemical detection of ascorbic acid, dopamine and uric acid, RSC Advances, 5(2015) 106307-14.

[55] C.e. Zou, J. Zhong, J. Wang, Y. Shiraishi, S. Li, B. Yan, et al., Fabrication of reduced graphene oxide–bimetallic Pd@Au nanocomposites for simultaneous determination of ascorbic acid, dopamine and uric acid, RSC Advances, 6(2016) 92502-9.

[56] H. Wang, L.-G. Xiao, X.-F. Chu, Y.-D. Chi, X.-T. Yang, Rational Design of Gold Nanoparticle/graphene Hybrids for Simultaneous Electrochemical Determination of Ascorbic Acid, Dopamine and Uric Acid, Chinese Journal of Analytical Chemistry, 44(2016) e1617-e25.

[57] D. Zhao, G. Yu, K. Tian, C. Xu, A highly sensitive and stable electrochemical sensor for simultaneous detection towards ascorbic acid, dopamine, and uric acid based on the hierarchical nanoporous PtTi alloy, Biosens Bioelectron, 82(2016) 119-26.

[58] P.L. dos Santos, V. Katic, K.C.F. Toledo, J.A. Bonacin, Photochemical one-pot synthesis of reduced graphene oxide/Prussian blue nanocomposite for simultaneous electrochemical detection of ascorbic acid, dopamine, and uric acid, Sensors and Actuators B: Chemical, 255(2018) 2437-47.

Acknowledgments

Resume of Team Member

Tianchen Liu (Leo)
Nanjing Foreign Language School, Nanjing 210008, PR China
+86 13305150026
3315863378@qq.com
Personal Data:
Sex: Male Date of Birth: Nov. 30, 2002
Birthplace: Nanjing, China

Zichen Yuan
Nanjing Foreign Language School, Nanjing 210008, PR China
+86 13913036107
2692321433@qq.com
Personal Data:
Sex: Female Date of Birth: Jun. 7, 2003
Birthplace: Nanjing, China

Hanqi Mo
Nanjing No.1 Middle School, Nanjing 210001, PR China
+86 15366110165
1624985614@qq.com
Personal Data:
Sex: Female Date of Birth: Nov. 20, 2003
Birthplace: Nanjing, China

Resume of Instructor

Liangliang Xu

Nanjing Foreign Language School, Nanjing 210008, PR China

+86 13605165763

njuxuliangliang@163.com

Graduated from the School of Chemistry and Chemical Engineering of Nanjing University in 2006 with a master's degree in polymer science.

Dr. & Professor Xiaojun Chen

College of Chemistry and Molecular Engineering, Nanjing Tech University, Nanjing 211800, PR China

+86 13813954619

chenxj@njtech.edu.cn

In 1995 and 2002, she obtained a bachelor's degree and a master's degree from Suzhou University respectively. In 2008, she obtained a doctorate degree in analytical chemistry from Nanjing University. In 2013-2014, she was an academic visitor in Oxford University. Her research field includes the assembly and construction of functional nanomaterials and electrochemical biosensors fabrication.

本参赛团队声明所提交的论文是在指导老师指导下进行的研究工作和取得的研究成果。尽本团队所知，除了文中特别加以标注和致谢中所罗列的内容以外，论文中不包含其他人已经发表或撰写过的研究成果。若有不实之处，本人愿意承担一切相关责任。

参赛队员：刘天辰 袁子晨 莫晗琦 指导老师：许嘉文 陈晓君

2019 年 09 月 15 日